© 2015. Published by The Company of Biologists Ltd | Development (2015) 142, 303-313 doi:10.1242/dev.110767

RESEARCH ARTICLE

STEM CELLS AND REGENERATION

Postnatal subventricular zone progenitors switch their fate to generate neurons with distinct synaptic input patterns

Namasivayam Ravi[1,2], Zhijun Li[2], Lars-Lennart Oettl[1,2], Dusan Bartsch[1], Kai Schönig[1] and Wolfgang Kelsch[1,2,*]

ABSTRACT

New granule cell neurons (GCs) generated in the neonatal and adult subventricular zone (SVZ) have distinct patterns of input synapses in their dendritic domains. These synaptic input patterns determine the computations that the neurons eventually perform in the olfactory bulb. We observed that GCs generated earlier in postnatal life had acquired an 'adult' synaptic development only in one dendritic domain, and only later-born GCs showed an 'adult' synaptic development in both dendritic domains. It is unknown to what extent the distinct synaptic input patterns are already determined in SVZ progenitors and/or by the brain circuit into which neurons integrate. To distinguish these possibilities, we heterochronically transplanted retrovirally labeled SVZ progenitor cells. Once these transplanted progenitors, which mainly expressed Mash1, had differentiated into GCs, their glutamatergic input synapses were visualized by genetic tags. We observed that GCs derived from neonatal progenitors differentiating in the adult maintained their characteristic neonatal synapse densities. Grafting of adult SVZ progenitors to the neonate had a different outcome. These GCs formed synaptic densities that corresponded to neither adult nor neonatal patterns in two dendritic domains. In summary, progenitors in the neonatal and adult brain generate distinct GC populations and switch their fate to generate neurons with specific synaptic input patterns. Once they switch, adult progenitors require specific properties of the circuit to maintain their characteristic synaptic input patterns. Such determination of synaptic input patterns already at the progenitor-cell level may be exploited for brain repair to engineer neurons with defined wiring patterns.

KEY WORDS: Adult neurogenesis, Synaptic development, Fate determination, Subventricular zone, Rat

INTRODUCTION

New neurons are continuously added to the adult mammalian brain. The most abundantly adult-generated neurons are granule cells (GC) in the olfactory bulb (OB). GCs are generated in the subventricular zone (SVZ) and integrate both into the developing (neonatal) and adult OB (Lois and Alvarez-Buylla, 1994). They are axon-less interneurons with an apical and a basal dendrite (Mori, 1987; Kelsch et al., 2010). The apical dendrite contains two domains (Fig. 1A). The proximal domain is an initial segment of the unbranched apical dendrite that receives axodendritic glutamatergic input synapses similar to the basal dendrite (basal domain). The distal domain starts after the first branch point of the apical dendrite. In the distal domain, GCs form reciprocal synapses with OB′ projection neurons that contain functionally coupled glutamatergic input and GABAergic output synapses (Hinds and Hinds, 1976).

Adult-born GCs differ in several features from neonatal-born GCs. Adult-born GCs acquire first synapses in the proximal domain and later in the distal domain (Whitman and Greer, 2007; Kelsch et al., 2008; Bardy et al., 2010). By contrast, neonatal-born neurons acquire synapses simultaneously in the proximal and distal domain (Kelsch et al., 2008). Adult-born GCs reach higher densities of glutamatergic synapses in the proximal domain than do neonatal-born neurons (Kelsch et al., 2008; Panzanelli et al., 2009). Neonatal- and adult-born neurons also respond differently to sensory deprivation (Kelsch et al., 2012), have different survival rates (Lemasson et al., 2005), and neonatal- but not adult-born neurons have slow presynaptic inhibition (Valley et al., 2013). Differences in the number of synaptic inputs in the dendritic domains determine the computations that GCs will eventually perform in the circuit (Lepousez et al., 2013). For example, the number of synapses in the distal domain influences the number of OB′ projection neurons to which the GC provides recurrent inhibition. By contrast, glutamatergic inputs to the proximal domain emerge from the olfactory cortices and modulate GC inhibition during olfactory processing (Yokoyama et al., 2011; Soria-Gómez et al., 2014). We therefore examined the domain-specific synaptic densities that GCs form at the end of their maturation.

Recent studies have revealed an unexpected degree of diversity in the intrinsic programs that determine neurotransmitter fate and cell type-specific connectivity of neurons derived from adult stem cells (Rakic et al., 2009; Ming and Song, 2011; Weinandy et al., 2011). It is an unanswered question whether GCs adopt the synaptic input patterns typical of the host circuit in which they integrate. Or, the differences in the synaptic input patterns in neonatal- and adult-born GCs may be an intrinsic property determined already in their neuronal progenitors. If so, progenitors proliferating at different times in the animal's life may generate GCs that do not revert their synaptic input patterns when challenged by heterochronic grafting.

We found that the synaptic input patterns are determined to a surprising extent already in progenitors. This determination progressively switched from neonatal to adult progenitors to generate characteristic synaptic input patterns of their neuronal offspring. These results provide evidence that neonatal and adult-born neurons originate from two progenitor populations that give rise to neurons with distinct synaptic input patterns.

RESULTS

Transition of synaptic development in postnatal life

During their synaptic maturation, adult-born GCs form higher densities of synapses in the proximal domain than in neonatal-born GCs. In the distal domain, neonatal- and adult-born GCs eventually reach similar synaptic densities. However, adult-born GCs form synapses in the distal domain later than neonatal-born GCs (Whitman

[1]Central Institute of Mental Health, Medical Faculty Mannheim, Heidelberg University, Mannheim 68159, Germany. [2]German Cancer Research Center, Heidelberg 69120, Germany.

*Author for correspondence (kelsch@uni-heidelberg.de)

Received 16 October 2014; Accepted 17 November 2014

Development (2015) 142, 303-313 doi:10.1242/dev.110767

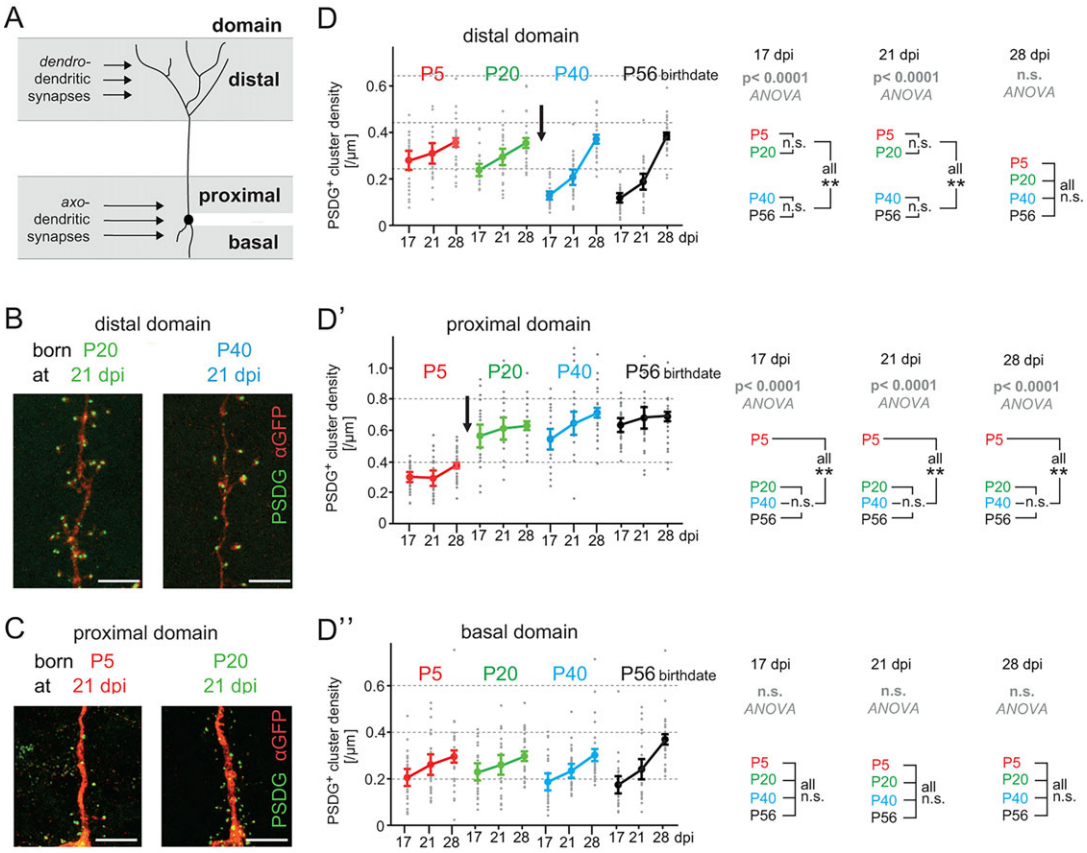

Fig. 1. Stepwise transition of the synaptic development from neonatal- to adult-born GCs. (A) Scheme of the dendritic domains of GCs. (B,C) GC progenitors were infected with an oncoretrovirus for PSDG expression at different postnatal days (P5, P20, P40) in the SVZ. In the distal domain (B), the switch from 'neonatal' to 'adult'-like PSDG$^+$ cluster densities occurred between P20- and P40-generated GCs, whereas in the proximal domain (C) the switch had occurred already between P5- and P20-generated GCs at 21 dpi. Scale bars: 10 µm. (D-D′) Development of PSDG$^+$ cluster densities (mean±s.e.m.) in the (D) distal, (D′) proximal and (D′) basal domain at 17, 21 and 28 dpi that were either born at P5, P20, P40 or P56 (*n*=23-25 GCs for each plotted data point). Right: separate statistical comparison for each dpi [ANOVA and post-hoc test (**P<0.001)].

and Greer, 2007; Kelsch et al., 2008; Bardy et al., 2010). We used these developmental differences to determine when GCs born between postnatal day (P)5 and adult age at P56 would change from a 'neonatal' to an 'adult' synaptic development in the two domains.

We labeled GC progenitors in the SVZ with replication-deficient oncoretroviruses. Oncoretroviruses have a short half-life and can only infect dividing progenitors (Sanes, 1989), thus enabling birth-dating of newly generated neurons. To visualize glutamatergic input synapses in the dendritic tree of single neurons, we expressed a genetic synaptic marker, PSDG, in GCs (Fig. 1). PSDG is a fusion protein between PSD-95 and GFP. PSD-95 is a protein localized to the postsynaptic density of glutamatergic input synapses (Sheng, 2001).

We infected GC progenitors in the SVZ with an oncoretrovirus encoding PSDG at P5, P20, P40 and P56 (Fig. 1). We examined GCs during the main period of synaptogenesis between 17 and 28 days post infection (dpi) when the differences in the distal and proximal domain are prominent between P5 and P56 generated GCs. The dendritic morphology of GCs was revealed by amplification of the low levels of diffusely distributed PSDG in the cytoplasm with antibodies raised against GFP, thus allowing measurements of synaptic densities in each of the dendritic domains. We observed that GC born at P20 had already switched to an 'adult' synaptic development in the proximal, but not in the distal domain (Fig. 1). In contrast to the proximal domain, the switch to an 'adult'-like synaptic development occurred later in the distal domain. The complete adult pattern was observed only in GCs generated at P40.

Grafting of GC progenitors

Based on the above observations, we performed heterochronic grafting to determine whether the eventual differences in synaptic input patterns resides in the specialized properties of neonatal and adult progenitors or in the mature versus immature OB environment. After a waiting period of 24 h, labeled GC progenitors were transplanted either isochronically [from adult to adult SVZ (A→A) or neonatal to neonatal SVZ (N→N)] or heterochronically [from adult to neonatal SVZ (A→N) or neonatal to adult SVZ (N→A)]. Direct grafting of the labeled progenitors to the host SVZ was chosen to minimize the influence of *in vitro* cell culture with removal of epigenetic markings or accumulation of genetic aberrations (Suhonen et al., 1996; Gabay et al., 2003; Maitra et al., 2005; Mekhoubad et al., 2012).

We first confirmed that our transplantation procedure did not produce carry-over of virus that could infect dividing progenitors in the host. In transgenic donor rats expressing β-Gal ubiquitously, we infected GC progenitors with a retrovirus encoding nuclear (NLS) mCherry (Fig. 2A-A″). Without transplantation, retrovirally labeled GCs in transgenic rats migrated from the SVZ to the GC layer of the OB, where 99.5% of mCherry$^+$ cells also expressed β-Gal at 14 dpi (*n*=679 GCs). When labeled GC progenitors from the donor transgenic SVZ were transplanted to the SVZ of wild-type (non-

Development (2015) 142, 303-313 doi:10.1242/dev.110767

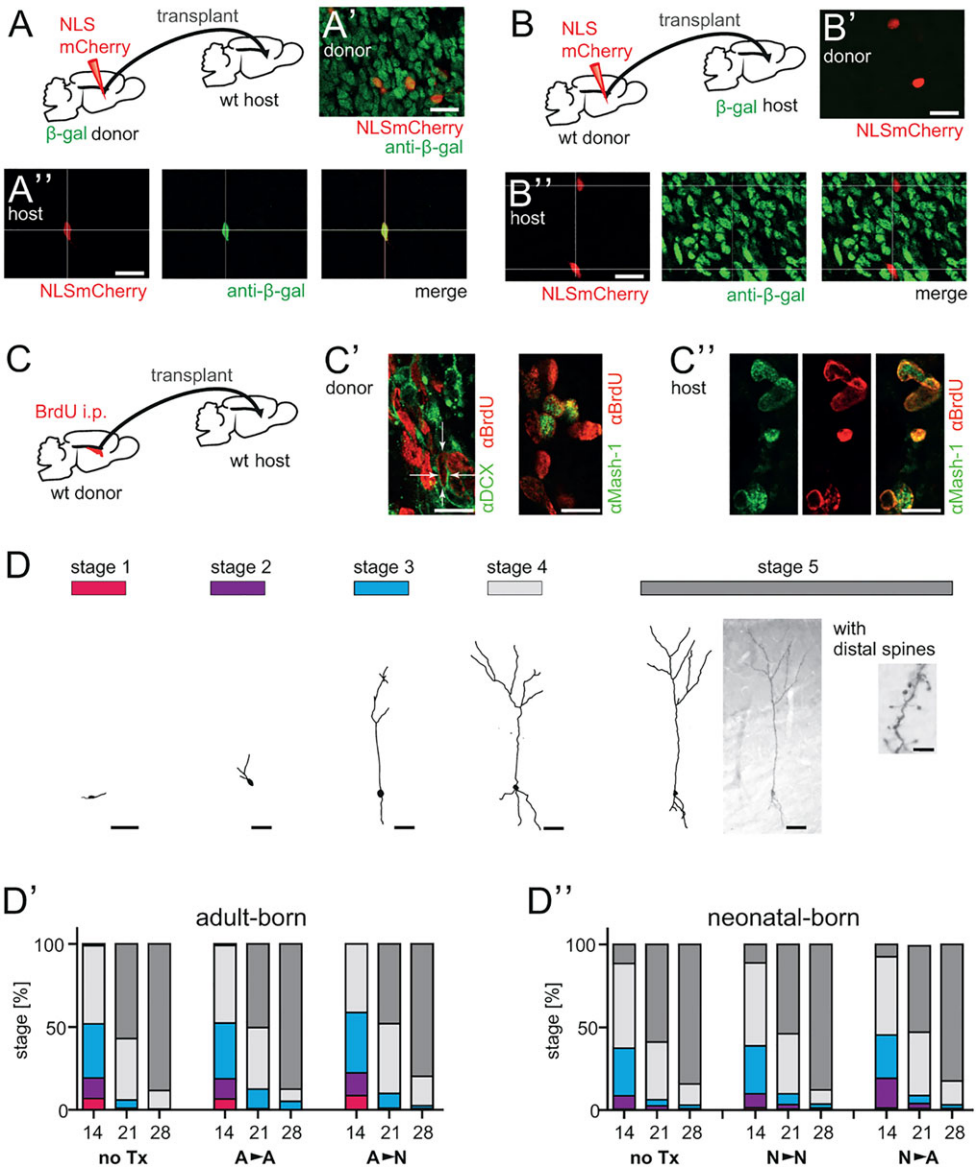

Fig. 2. Transplanted GC progenitors originate from the donor SVZ. (A-A″) To confirm that retrovirally labeled GCs originated from donor rats, a retrovirus encoding NLSmCherry$^+$ was injected in the SVZ of transgenic donor rats expressing β-Gal ubiquitously. After a waiting period of 24 h, SVZ progenitors were transplanted to the SVZ of wild-type rats (A). (A′) Control condition: non-transplanted mCherry$^+$ β-Gal$^+$ GCs in the GC layer of the donor OB at 14 dpi. (A″) mCherry$^+$ β-Gal$^+$ GCs after transplantation in the GC layer of the wild-type host OB (N→N) at 14 dpi. Scale bars: 20 µm. (B-B″) To test for fusion of retrovirally labeled donor with host cells (N→N), a retrovirus encoding NLSmCherry$^+$ was injected into the SVZ of wild-type rats. After a waiting period, SVZ progenitors were transplanted to the SVZ of transgenic host rats expressing β-Gal ubiquitously (B). (B′) Control condition: non-transplanted mCherry$^+$ β-Gal$^-$ cell in the GC layer of the donor OB at 14 dpi. (B″) mCherry$^+$ GCs in the transgenic host GC layer were β-Gal$^-$ at 14 dpi. Scale bars: 20 µm. (C) To determine the types of progenitor cells that were transplanted to the host SVZ, a cell-division marker BrdU (100 mg/kg bodyweight) was injected instead of the retrovirus into donor rats (C). Expression of Mash1 and DCX was examined in BrdU$^+$ SVZ cells in non-transplanted littermates that were sacrificed at the same time as the transplanted rats (C′). (C″) Mash1 expression in BrdU$^+$ SVZ cells after transplantation. Scale bars: 10 µm. (D-D″) The morphological differentiation was assessed according to stages 1-5 (D), shown here for A→A GCs retrovirally labeled with membrane-tagged GFP. Stage 1, tangentially migrating neuroblasts; stage 2, radially migrating young neurons; stage 3, GCs with a simple unbranched dendrite that does not extend beyond the mitral cell layer; stage 4, GCs with a branched dendrite in the external plexiform layer, but with few spines; stage 5, mature GCs with densely spined distal dendrites. Scale bars: 50 µm, except images of spines (5 µm). Percentages of stage 1-5 GCs at 14, 21 and 28 dpi for non-transplanted (no Tx) and transplanted precursors originating from the adult (D′) and neonatal SVZ (D″) (n=744-1056 GC for no Tx and n=96-163 transplanted GCs for each time-point).

transgenic) hosts, 99.3% of mCherry$^+$ GCs were also β-Gal$^+$ in the GC layer of the OB at 14 dpi (n=542 GCs). These observations indicate that our procedure selectively labeled progenitors from the donor SVZ, and that there was no viral carry over that labeled progenitors in the host SVZ.

We also tested whether fusion of donor cells with host cells contributed to the labeling of cells in the host OB. We transplanted mCherry$^+$ SVZ cells from wild-type rats to the SVZ of rats expressing β-Gal ubiquitously. In this experiment, cell fusion would give rise to GCs that express both the retroviral marker mCherry and the transgene β-Gal. Only one of 552 mCherry$^+$ GCs also expressed β-Gal in the transgenic hosts (at 14 dpi, n=12 host rats; Fig. 2B-B″), indicating that cell fusion was a rare event.

Development (2015) 142, 303-313 doi:10.1242/dev.110767

To determine the type of transplanted progenitor cell that was predominantly found in the host SVZ, we repeated the N→N grafting experiment under the same conditions, but instead of retroviral infection we used i.p. injection of BrdU (100 mg/kg body weight). BrdU, like oncoretroviruses, labels cells during cell division. Oncoretroviruses, however, need up to several days for robust expression of marker proteins (mCherry), whereas BrdU is immediately detectable. Twenty four hours after BrdU labeling, we transplanted SVZ cells and examined the host SVZ 6 h after grafting. In the host SVZ, out of the 416 $BrdU^+$ cells, 98.9% expressed Mash1 (Ascl1), a marker for fast-amplifying progenitors, whereas only 16 out of 447 $BrdU^+$ cells expressed doublecortin (DCX), a neuroblast marker (n=5 rats, Fig. 2C-C″). A control cohort of five littermate rats were injected with BrdU and examined without transplantation in parallel to the N→N group. Among these non-transplanted $BrdU^+$ SVZ cells, 44.8% had Mash1 colocalization and 33.3% expressed DCX (n=419 and 679 cells, respectively, Fig. 2C-C″). These observations suggest that our transplantation procedure resulted in the selection of $Mash1^+$ fast-amplifying progenitor cells.

Next, we examined the morphological differentiation of grafted GCs. GC progenitors were infected in the host with a retrovirus delivering a membrane-bound GFP that visualized their entire dendritic arbor. Iso- and heterochronically grafted or non-transplanted GCs derived from adult progenitors reached stages of their morphological maturation at the same dpi and eventually had dendritic trees of similar size (Fig. 2D-D″, supplementary material Fig. S1). In addition, GCs derived from neonatal progenitors were relatively consistent when comparing the respective grafting conditions. Notably, GCs derived from neonatal and adult progenitors differed in the fraction of migrating cells at 14 dpi. This latter difference persisted after heterochronic grafting. After 14 dpi, however, no significant differences were detected between GCs derived from neonatal and adult progenitors. These observations suggest that early differences in the migration of GCs derived from neonatal and adult progenitors exist that are independent of the environment in which they differentiate.

To also test whether transplanted progenitors give rise to neurons with normal physiological properties, we performed targeted whole-cell recordings from N→N or non-transplanted neonatal-born GCs. Retroviral labeling with mCherry was performed as described in Fig. 3A. At 28-32 dpi, transplanted and non-transplanted GCs developed spontaneous synaptic glutamatergic inputs (sEPSCs) of similar frequencies and amplitude (n.s., Mann-Whitney test, n=15 GCs, respectively; Fig. 3A-B′), as well as comparable action-potential discharge upon current injection in N→N and non-transplanted GCs (n=15 GCs, respectively; n.s., ANOVA; Fig. 3C,D). In addition, the resting membrane potential (mean±s.e.m.: −68.5±1.6 mV and −70.4 ±2 mV), the membrane resistance (1.1±0.2 GΩ and 1.0±0.1 GΩ), and the membrane capacitance (7.0±0.5 pF and 7.6±0.5 pF) were similar in N→N and non-transplanted GCs, respectively (all n.s., t-test, n=15 cells), indicating that transplanted progenitors gave rise to GCs that integrated appropriately into the host circuit.

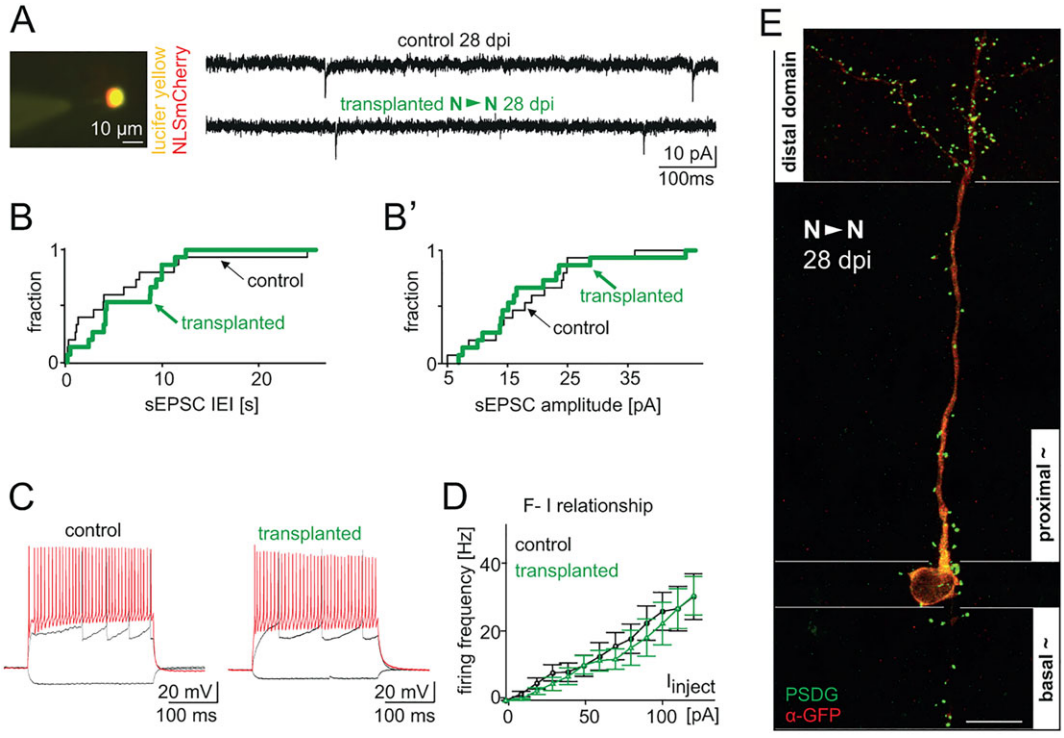

Fig. 3. Transplanted GCs develop normal synaptic inputs. (A) Recording of sEPSCs with a pipette containing lucifer yellow (left) of either $mCherry^+$ non-transplanted (control) or transplanted (N→N) GCs in the presence of gabazine (10 µM) at 28 dpi (V_h=−70 mV). (B,B′) Cumulative distribution of the sEPSC inter-event intervals (IEI) (B) and amplitudes (B′) of $mCherry^+$ control or transplanted (N→N) GCs (n=15 cells, respectively) at 28-32 dpi (data are not significantly different, Mann-Whitney test). (C) Action potential discharge patterns upon intracellular current injection (−20, 50 and 140 pA for 500 ms) of the GCs shown in A. (D) Plot of the action potential firing frequency against the injected current (I_{inject}) (mean±s.e.m.) in $mCherry^+$ control or transplanted GCs at 28-32 dpi (data are not significantly different, ANOVA, n=15 same neurons as shown in B). (E) Maximum density projection of confocal stacks taken from a N→N GC at 28 dpi with a retrovirus expressing PSDG. $PSDG^+$ clusters were detected by direct intrinsic fluorescence (green). The dendritic morphology of the GC was revealed by amplification of the low levels of diffusely distributed PSDG in the cytoplasm with immunofluorescence against GFP (red). Scale bar: 10 µm.

Development (2015) 142, 303-313 doi:10.1242/dev.110767

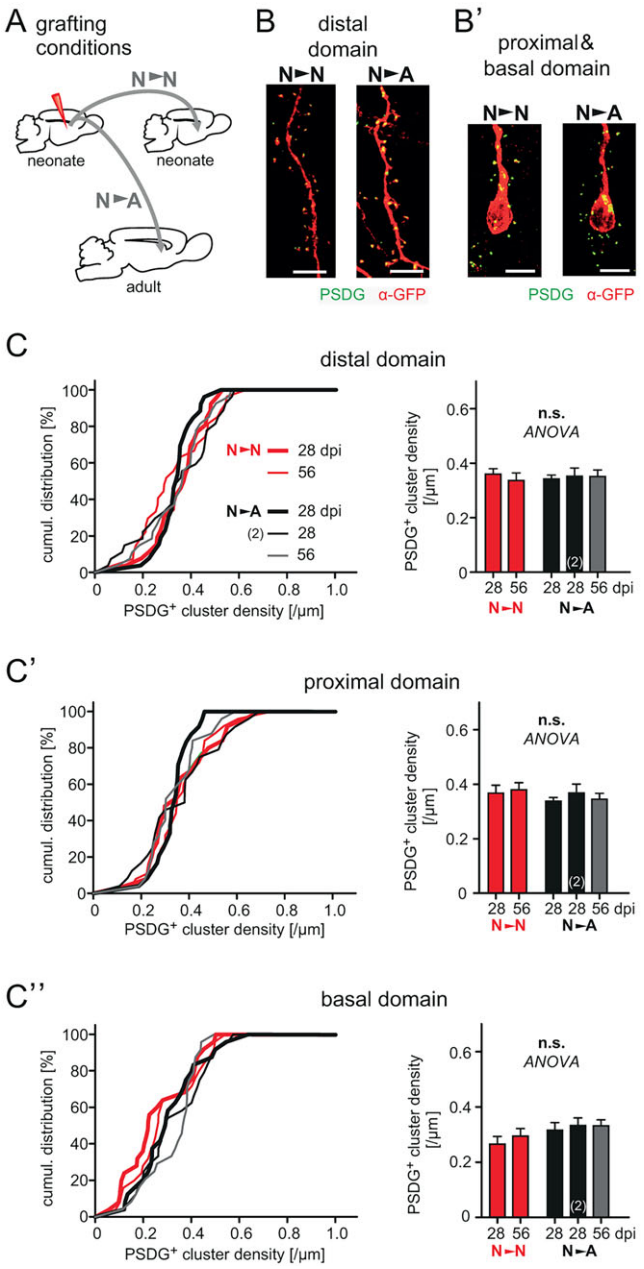

Fig. 4. Synaptic input patterns of GCs derived from neonatal progenitors. (A) Neonatal progenitors were simultaneously grafted either to the host neonatal (N→N) or adult SVZ (N→A). (B,B′) Maximum density projection of the (B) distal, and (B′) proximal and basal domain from PSDG$^+$ N→N and N→A GCs at 28 dpi. Scale bars: 10 µm. (C-C″) Cumulative plots of PSDG$^+$ cluster densities for N→N and N→A GCs at 28 and 56 dpi in the (C) distal, (C′) proximal and (C′) basal domain (n=23-25 GCs for each plotted data point). To test for consistency of the observed pattern of synaptic development upon transplantation, we repeated the N→A transplantations with a second blinded experimenter and replicated the same pattern '(2)'. Right: statistical comparison (mean±s.e.m.) of the data shown on the left (ANOVA).

Grafting of neonatal GC progenitors

We then examined the pattern of PSDG$^+$ input synapses of neonatal-born GCs upon grafting of their progenitors (Figs 3E and 4). Only before 17 dpi, differences in the stage of dendritic outgrowth were detectable between GCs derived from neonatal and adult progenitors (Fig. 2D-D″). Hence, we focused on GCs at 28 and 56 dpi when they had reached their final synaptic densities. The N→N GCs acquired the same densities of PSDG$^+$ clusters in their dendritic domains as non-transplanted neonatal-born GCs (supplementary material Fig. S2). Surprisingly, N→N and N→A GCs developed the same PSDG$^+$ synapse densities in their dendritic domains (Fig. 4B-C″). Neonatal-born GCs have lower densities of synapses in the proximal domain than do adult-born GCs (Kelsch et al., 2008). Comparable with non-transplanted neonatal-born cells, N→A GCs maintained lower densities of the proximal synapses than in A→A GCs (at 28 and 56 dpi: P<0.001, t-test, respectively, for comparison of data from Figs 4C′ and 5C′), further supporting the observation that N→A GCs retained their neonatal synaptic input patterns. Furthermore, in the distal domain, the glutamatergic input synapse is colocalized and functionally coupled with an inhibitory output synapse. To analyze densities of these output synapses, we used SypG, a synaptophysin-GFP fusion protein. Synaptophysin is a protein that is localized to presynaptic neurotransmitter vesicles and SypG expressed with retroviral vectors can be used to label output synapses genetically (Meyer and Smith, 2006; Kelsch et al., 2008). In line with coupled input and output synapses in the distal domain, N→N and N→A GCs had similar densities of SypG$^+$ clusters (supplementary material Fig. S2B). These observations reveal that the synaptic input patterns of neonatal-born GCs are an intrinsic property that is maintained independently of whether they differentiated in a mature or immature OB.

Grafting of adult GC progenitors

We then examined the pattern of PSDG$^+$ input synapses of adult-born GCs upon grafting of their progenitors (Fig. 5). A→A GCs maintained the synapse densities of non-transplanted adult-born GCs (supplementary material Fig. S3) with higher PSDG$^+$ cluster densities in their proximal domain than N→N GCs (at 28 and 56 dpi: P<0.001, t-test, respectively, for comparison of data from Figs 4C′ and 5C′).

We analyzed the densities of PSDG$^+$ synapses in the dendritic domains of A→N GCs at 28 and 56 dpi (Fig. 5B-C″). In the distal and proximal domains, A→N GCs failed to reach the densities of PSDG$^+$ clusters characteristic of A→A GCs. In addition, when compared with N→N GCs, the densities of PSDG$^+$ clusters of A→N GCs were significantly lower in the distal domain at 28 and 56 dpi (P<0.001, t-test, respectively, for comparison of data from Figs 4C and 5C). This latter observation indicates that adult-born GCs did also not adopt a 'neonatal' wiring pattern when they differentiated in the neonatal brain. Importantly, PSDG$^+$ clusters in the basal domain of A→N and A→A GCs reached similar densities (Fig. 5C″), suggesting that A→N GCs can still form normal synaptic densities in at least one domain. In the distal domain, A→N and non-transplanted GCs had their PSDG$^+$ clusters equally located in spines (supplementary material Fig. S4) and 97.4% of PSDG$^+$ clusters were contacted by a presynaptic protein, bassoon, at 28 dpi (n=346 synapses, Fig. 6A), supporting the observation that PSDG in transport vesicles did not significantly contribute to the detected PSDG$^+$ clusters of mature GCs and that genetically tagged PSDG$^+$ clusters represented bona fide synapses. Consistent with reduced densities of glutamatergic input in the distal domain, the density of spine protrusions (Fig. 6B) and of SypG$^+$ output synapses (Fig. 6C) was also reduced in this domain of A→N compared with A→A GCs.

Properties of heterochronically grafted GCs

In the neonatal and adult SVZ, deep and superficial GCs are generated (Kelsch et al., 2007; Merkle et al., 2007), even though

Development (2015) 142, 303-313 doi:10.1242/dev.110767

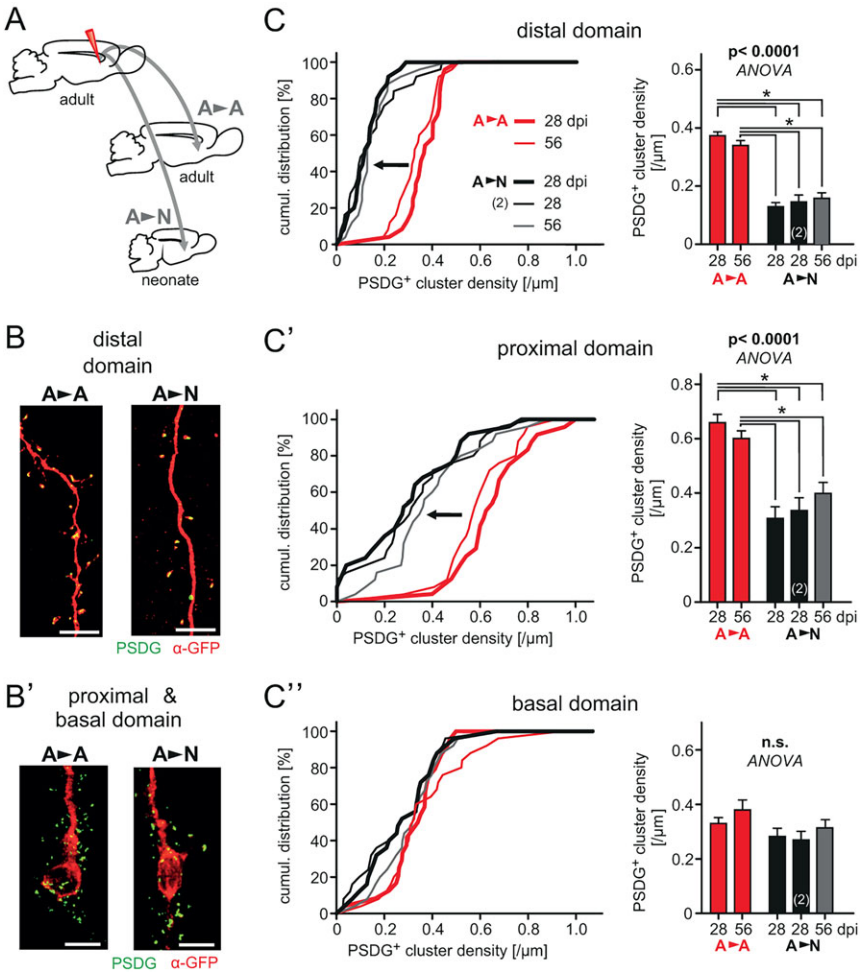

Fig. 5. Synaptic input patterns of GCs derived from adult progenitors. (A) Adult progenitors were simultaneously grafted either to the host adult (A→A) or neonatal SVZ (A→N). (B,B′) Maximum density projection of the distal (B), and proximal and basal (B′) domain of PSDG$^+$ A→A and A→N GCs at 28 dpi. Scale bars: 10 µm. (C-C′) Cumulative plots of PSDG$^+$ cluster densities for A→A and A→N GCs at 28 and 56 dpi in the distal (C), proximal (C′) and basal domain (C″) (n=23-25 GCs for each plotted data point). To test for consistency of the observed pattern of synaptic development upon transplantation, we repeated the A→N transplantations with a second blinded experimenter and replicated the same pattern '(2)'. Right: statistical comparison (mean± s.e.m.) of the data shown on the left [ANOVA and post-hoc test (*P<0.05)].

more deep cells are produced in adult animals (Lemasson et al., 2005). Both deep and superficial GCs switch from a 'neonatal' to an 'adult' synaptic input patterns while the animal grows up (Kelsch et al., 2008). In line with 'adult' synaptic input patterns in deep and superficial A→N GCs, both had the same reduced PSDG$^+$ cluster densities upon transplantations (Fig. 6D).

To examine the function of glutamatergic inputs to A→N GCs, we performed targeted whole-cell recordings from A→A and A→N GCs at 28-32 dpi (Fig. 6E) that had been virally labeled as described in Fig. 3A. Electrical stimulation in the GC layer was used to activate synaptic EPSCs in the perisomatic region followed by stimulation in the external plexiform layer to activate inputs to the distal domain. All recordings were performed with gabazine (10 µM) to prevent co-activation of inhibitory inputs. In A→N GCs, the amplitude of perisomatic inputs had faster rise times than did distal stimulation (0.98±0.15 and 4.38±0.65, respectively, in six GCs, P=0.0005, t-test). In addition, the decay times were faster for perisomatic inputs than for distal stimulation (4.35±1.02 and 17.6±2.59, respectively, in six GCs, P=0.0008, t-test) and sEPSCs were blocked by the AMPAR antagonist CNQX (10 µM) at the end of the recording (Fig. 6E). These results support the notion that, although their synaptic densities were reduced, A→N GCs still formed functional synapses. The rise times of proximal and distal EPSC inputs to 28- to 32-day-old A→A GCs were 1.07±0.17 and 4.13±0.52, respectively, in five GCs (P=0.0007, t-test), suggesting that the dendritic excitability was similar in A→A and A→N GCs as revealed by the comparison of the rise times of their respective perisomatic and distal glutamatergic inputs (both n.s., t-test).

Finally, we tested whether spine or synapse densities already differed between A→A and A→N GCs by 21 dpi. As described by Whitman and Greer (2007), the increase in spine density (Fig. 6B) preceded that of the increase in synapses revealed by synaptic marker proteins (Fig. 7). There was no significant difference in spine density between A→A and A→N GCs at 21 dpi, suggesting that the initial spine formation is preserved (Fig. 6B). In addition, the densities of glutamatergic synapses in the distal and proximal domain were comparable in A→A and A→N GCs at 21 dpi (Fig. 7). In the proximal domain, A→N GCs initially formed high densities of PSDG$^+$ synapses at 21 dpi (Fig. 7), that were lost during further maturation (28 dpi, Fig. 5), suggesting that synapse maturation rather than initial synapse formation is impaired after A→N transplantation.

DISCUSSION

This study revealed the influence of intrinsic properties of Mash1$^+$ progenitors on the formation of distinct synaptic input patterns, a feature central to synaptic wiring. In particular, GCs generated from neonatal progenitors maintained their 'neonatal' synaptic input patterns independently of whether they differentiated in a neonatal or adult circuit. However, GCs generated from adult progenitors differentiating in the neonate, developed neither a 'neonatal' nor an 'adult' synaptic input pattern. These findings support the finding that neonatal and adult progenitors generate GCs with distinct programs for the formation of synaptic input patterns.

Development (2015) 142, 303-313 doi:10.1242/dev.110767

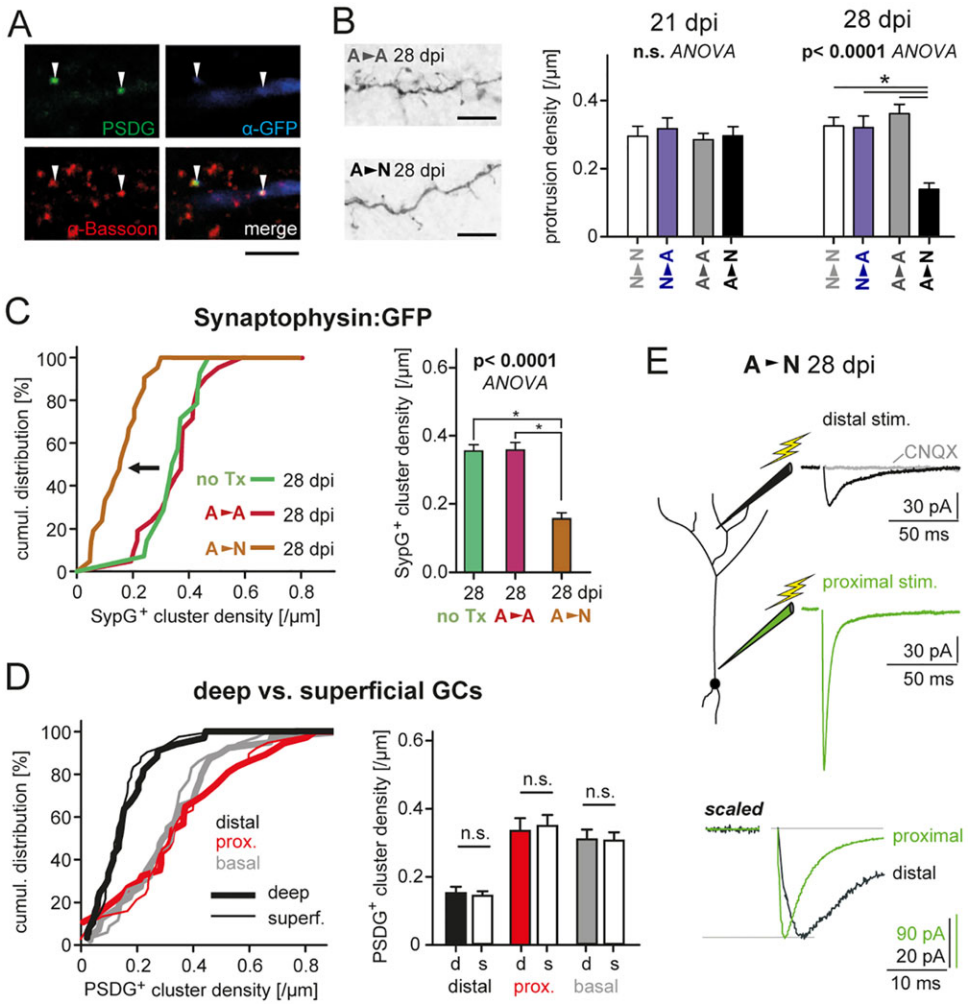

Fig. 6. Properties of synapses of GCs derived from adult progenitors. (A) Single confocal plane: PSDG$^+$ clusters (arrowheads) in an A→N GCs at 28 dpi were contacted by Bassoon$^+$ presynaptic sites (red immunofluorescence) at the dendrite and spines (blue immunofluorescence against GFP). Scale bar: 5 µm. (B) Spines in transplanted GCs were visualized with DAB immunohistochemistry against retrovirally delivered membrane-tagged GFP (left images). Scale bars: 10 µm. Right: quantification of spine-like protrusions in the distal domain (n=10 GCs for each transplantation condition and time point) [ANOVA and post-hoc test (*P<0.05)]. (C) Cumulative plots of SypG$^+$ clusters that label presynaptic output synapses in the distal domain of for A→A, A→N and non-transplanted (no Tx) adult-born GCs at 28 dpi (n=25, 25, 14 GCs, respectively). Right: statistical comparison (mean±s.e.m.) of the data shown on the left [ANOVA and post-hoc test (*P<0.05)]. (D) Cumulative plots of PSDG$^+$ cluster densities for pooled data of A→N GCs at 28 dpi in the distal, proximal and basal domains of the data shown in Fig. 5C. Pooled data were split into deep (d) and superficial (s) GCs. Deep GCs had to have a soma position in the lower 50% of the GC layer (for the basal and proximal domain) and the first branch point of the apical dendrite in the lower 50% of the external plexiform layer (for the distal domain). Right: statistical comparison (mean±s.e.m.) of the data shown on the left (t-test). (E) Electric stimulation in the distal and proximal domain of a 28 dpi A→N evoked CNQX-sensitive (10 µM) EPSCs with rise and decay times that were slow and fast, respectively, as also shown for amplitude-scaled EPSCs. Recordings were performed in the presence of gabazine (10 µM).

Heterochronic grafting of progenitors

We chose grafting of retrovirally labeled progenitors to address the role of circuit environment and intrinsic programs in the generation of different wiring patterns. Using this procedure, oncoretroviral infection only labeled cells from the donor, but not in the host SVZ, and cell-fusion of donor cells with host SVZ cells did not contribute to GCs in the host OB upon grafting. The grafted progenitors expressed Mash1, which is indicative of fast-amplifying progenitor cells. For direct comparison of the different grafting conditions, progenitors were grafted iso- and heterochronically from the same donor animal. The neuronal offspring of isochronically grafted progenitors maintained the timing of their maturation steps and developed functional synaptic densities similar to non-transplanted GCs.

We chose genetic synaptic tags as they allow quantification of synaptic densities in each dendritic domain of a single neuron. The differences in domain-specific input densities distinguish ‘neonatal’ and ‘adult’ wiring patterns. Recordings of synaptic events would also allow quantification of synapse numbers, but not attribution of inputs to specific domains such as basal or proximal inputs. Local synaptic stimulation or glutamate uncaging along the dendrite can be used to determine the site of input at the respective domain, but will not easily allow quantification of synapse densities. A potential concern related to overexpression of PSD-95 is that it has been demonstrated to induce plasticity of glutamatergic synapses (El-Husseini et al., 2000; Nikonenko et al., 2008; Taft and Turrigiano, 2014). For example in the work of El-Husseini et al. (2000), overexpression was tenfold higher than the endogenous PSD-95 level, while retroviral expression only doubled the endogenous

Development (2015) 142, 303-313 doi:10.1242/dev.110767

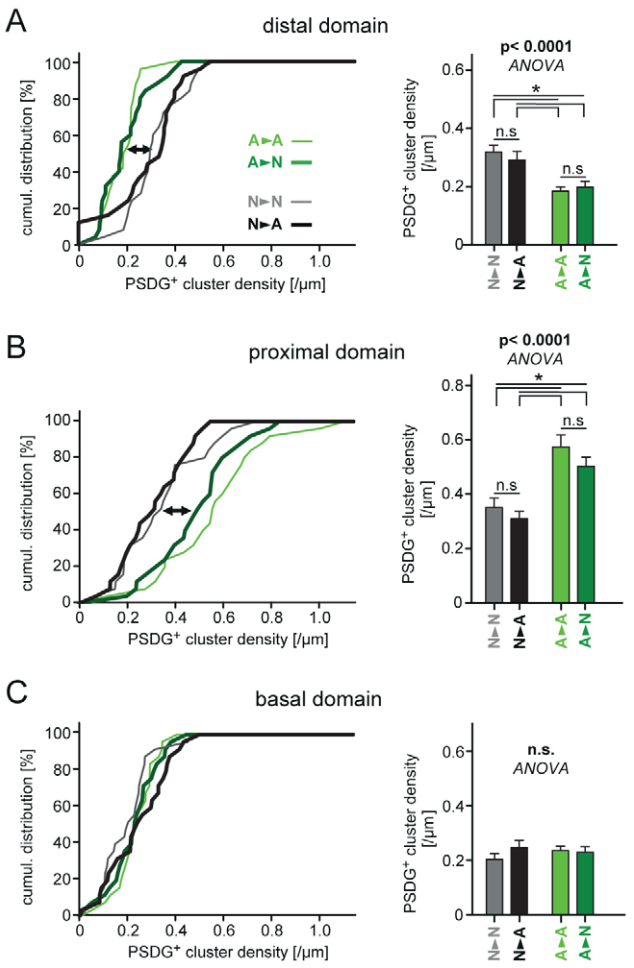

Fig. 7. Synaptic input patterns of GCs derived from neonatal and adult progenitors at 21 dpi. Cumulative plots of PSDG$^+$ cluster densities for all four transplantation conditions at 21 dpi in the distal (A), proximal (B) and basal domain (C) (n=23-25 GCs for each plotted data point). Right: statistical comparison (mean±s.e.m.) of the data shown on the left [ANOVA and post-hoc test (*P<0.05)].

neuronal PSD-95 content (Kelsch et al., 2008). This retroviral expression of PSDG does not alter the amplitude or frequency of glutamatergic synaptic inputs (Kelsch et al., 2008). In further support, two other readouts (i.e. the synaptic marker SypG and spine densities visualized by membrane-tagged GFP) revealed similar changes in PSDG$^+$ synapse densities.

The dendritic domains receive glutamatergic inputs from different neuron types and brain regions. The output of a neuron to the circuit depends on the number of synaptic inputs it forms with the different neuron types. In this study, we could infer from changes of synaptic densities that the numbers of synapses in a dendritic domain changed as the length of the dendrite remained stable upon iso- or heterochronic grafting.

Furthermore, N→A GCs maintained their lower 'neonatal' numbers of input synapses in the proximal domain compared with adult-born GCs. The proximal domain receives cortical inputs that globally excite GC and thereby boost dendrodendritic inhibition in the distal domain. Differences in the number of inputs to the proximal domain are therefore likely to impact GC inhibition during active olfactory processing and learning. In the distal domain, GCs usually form only one synaptic contact with each projection neuron dendrite (Woolf et al., 1991). Thus, A→N GCs, which had lower total numbers of synapses in the distal domain, are likely to innervate a lower number of projection neurons.

Intrinsic determination of synaptic input patterns

The specification of SVZ progenitors may not only dictate the neurotransmitter phenotype and the position of the neurons in different layers (Hack et al., 2005; Merkle et al., 2007; Rakic et al., 2009), but may also be linked to the formation of characteristic synaptic input patterns. This is supported by the finding that GC derived from neonatal progenitors maintained their characteristic synaptic input patterns regardless of whether they matured in the adult or neonatal circuit. Other features also persisted in the synaptic development. As previously described (Whitman and Greer, 2007), adult-born GCs first showed an increase in spine densities followed by the maturation of synapses, as revealed by synaptic marker proteins. Interestingly, this dissociation persisted after heterochronic grafting. Furthermore, N→A GCs also retained their typical early increase in synapse density in the distal domain, whereas these synapses formed late in adult-born GCs (A→A or non-transplanted). The observation that GCs derived from neonatal and adult progenitors retained their respective 'neonatal' and 'adult' wiring patterns upon grafting to the adult host revealed that the circuit itself permits for variable wiring patterns. These GCs originated from transplanted Mash1$^+$ fast-amplifying cells. Thus, at least at this stage progenitors are relatively committed to give rise to a specific synaptic input pattern. It is, however, very possible that at earlier stages, such as the slowly dividing stem cells, these properties are not yet determined. We had observed that GCs derived from neonatal and adult progenitors already differ in their migration and outgrowth of their dendrites. This difference persisted when the progenitors differentiated in a heterochronic environment. It is therefore possible that some of these early differences will, through yet unknown mechanisms, still influence the eventual synaptic patterns of GCs. Yet these differences in migration and the stages of dendritic outgrowth were detected only before 17 dpi.

Another feature of synaptic wiring is cell type-specific connectivity. Progenitors are determined to generate deep or superficial GCs that connect to one of two types of projection neurons (Kelsch et al., 2007; Merkle et al., 2007). These two types of projection neurons form independent subcircuits in the OB. The switch from 'neonatal' to 'adult' synaptic input patterns occurs both in deep and superficial GCs, suggesting that cell type-specific connectivity and synaptic input patterns are determined independently. These progenitor programs may provide a framework based on which activity-dependent plasticity can generate further variations in the synaptic input patterns depending on the animals' current environment.

Interaction of intrinsic determination and circuit environment

Grafting of adult progenitors also revealed a crucial role for the host circuit during the formation of synaptic input patterns. GCs originating from the same adult progenitors readily completed their characteristic synaptic input patterns in their isochronic (adult), but not in a heterochronic (neonatal) OB. Importantly, GCs derived from adult progenitors neither maintained their characteristic 'adult' synaptic densities, nor did they adopt the fate typical of neurons in the 'neonatal' host OB. Compatible with this finding, it has been shown that certain molecules are upregulated in the adult OB, such as tenasin-R, which influences the maturation of adult- but not neonatal-born GCs (David et al., 2013).

Interestingly, heterochronic grafting of adult progenitors resulted in GCs with reduced synapse densities both in the distal and

Development (2015) 142, 303-313 doi:10.1242/dev.110767

proximal domain. We now observed that GCs generated at different times in postnatal life switched from 'neonatal' to 'adult' formation of synaptic input patterns independently in the proximal and distal domain. The switches from 'neonatal' to 'adult' patterns did not revert, as revealed by heterochronic grafting of adult progenitors. These observations provide further evidence that adult neurogenesis is not a simple continuum of neurogenesis during brain development. As neonatal- and adult-born GCs also differ in other properties of their synaptic organization (Kelsch et al., 2009; Nissant et al., 2009; Bardy et al., 2010; Valley et al., 2013), future studies may address whether these differences also arise from switches in the progenitor fate.

The intrinsic properties of progenitor cells controlling synaptic wiring may need to be considered for repair strategies. In particular, neural stem cells appear to be specified to generate interneurons that cannot be easily converted towards generating of other neuronal subtypes (Weinandy et al., 2011). It will be crucial to determine whether synaptic input patterns are determined only at the fast-amplifying progenitor stage or already at the level of slowly dividing stem cells. Taking into consideration the limited adaptability of intrinsic properties of neuronal progenitors, the repair of brain circuits by neuronal replacement strategies may require engineering of neuronal precursors to produce new neurons that match the properties of the target circuit.

MATERIALS AND METHODS

Animals and husbandry

Adult female (>P56) and neonatal (P5) Sprague-Dawley rats were obtained from Charles River and housed in groups of three or four adult female rats under standard conditions at a 12 h day/night cycle. Pups were weaned at P28. All procedures were approved by the local animal welfare committee (RP Karlsruhe, permission number 35-9185.81/G-186/10) and in accordance with NIH guidelines. Transgenic reporter rats$^{CAG\text{-}loxP.LacZ.STOP.loxP\text{-}EGFP}$ with ubiquitous expression of nuclear localized (NLS) β-Gal (Schönig et al., 2012) were bred in a Sprague-Dawley background.

Retroviruses

Oncoretroviral vectors derived from Moloney Leukemia virus with an internal promoter derived from the LTR from the Rous Sarcoma Virus (RSV) were generated by replacing the membrane-bound (palmitoylated) GFP with the open reading frame of PSDG or SypG to visualize glutamatergic postsynaptic clusters or presynaptic release sites, respectively, or NLSmCherry. Recombinant virus was prepared and stored as described previously (Lois et al., 2002). The viral titer was 10^6-10^7 infectious units/µl.

Stereotactic surgery and transplantation procedure

Adult animals were anesthetized with isoflurane and neonatal animals by hypothermia. We initially compared different anesthesia methods. Using either hypothermia or ketamine/xylazine compared with isoflurane anesthesia for neonatal and adult rats, respectively, had no effects on the maturation of synaptic densities, but lethality was higher in neonates for isoflurane compared with hypothermia. Rats were stereotactically injected with a retrovirus bilaterally into the SVZ. The SVZ coordinates were (in mm relative to Bregma): anterior 1.2, lateral 1.6, ventral 3.1 for adult rats, and anterior 0.9, lateral 2.1, ventral 2.1 for neonatal rats (supplementary material Fig. S1A). To maximize the yield of transplanted labeled GCs, we injected 1 µl of retrovirus per side, thus resulting in widespread infection in the SVZ containing both deep and superficial GCs. After surgery, neonatal animals were returned to their mother. Alternatively, in the experiments shown in Fig. 2C-C″, BrdU (100 mg/kg BW) was injected i.p. 24 h before transplantation. After a waiting period of 24 h, rats with retroviral labeling in the SVZ were killed by an overdose of isoflurane, immediately decapitated, their brains removed and placed in sterile phosphate-buffered saline (PBS without Ca^{2+} and Mg^{2+}, pH 7.2) at room temperature (25°C). Brains were cut into coronal slices with a razor blade and the SVZ zone was dissected and cut into small pieces under a stereomicroscope. After transfer to a 1.5 ml vial, the tissue was gently dissociated by repeated pipetting and back loaded into a glass capillary for stereotactic injection. The animals were prepared for stereotactic injections as described above and the dissociated tissue was injected into the SVZ with the same coordinates as described for retroviral injections. Tissue from the same donor (e.g. neonate) was simultaneously transplanted iso- and heterochronically to minimize differences between the transplantation conditions. The tissue was directly transplanted upon dissociation, cell numbers were not counted to minimize the time between dissection and injection of cells into the host SVZ. Approximately half of the host OBs contained labeled GCs and their numbers ranged between approximately tens to a few hundred of cells per bulb. After surgery, animals were returned to their home cage. The procedure was optimized so that the time from decapitation of the donor rat to injection of the host rats did not exceed 15 min.

Histology

The animals were euthanized with an overdose of isoflurane followed by transcardiac perfusion with PBS at 35°C for 30 s and subsequently paraformaldehyde (4% in PBS, Roth) at room temperature for 3 min. Brains were removed and post-fixed in paraformaldehyde overnight. Coronal sections (50 µm) were prepared with a vibratome. For visualization of genetic synaptic markers, tissue sections were incubated in rabbit anti-GFP primary antibody (1:10,000, Millipore) diluted in blocking solution containing PBS, 0.3% Triton X100 and 1% bovine serum albumin at 4°C overnight. Sections were washed three times in PBS and then incubated with Cy-3 conjugated anti-rabbit secondary antibody (1:1500, Jackson ImmunoResearch) in blocking solution at room temperature for 2 h. Sections were again washed three times in PBS and mounted on slices with Gelmount (Sigma). For labeling of presynaptic sites, mouse anti-Bassoon (1:1000, VAM-PS003, Enzo Life Science) and rabbit anti-GFP primary (1:10,000) and A555-conjugated anti-mouse (1:1000, Molecular Probes) and Cy5-conjugated anti-rabbit (1:1500, Jackson ImmunoResearch) secondary antibodies were used. For control experiments using β-Gal reporter rats, anti-rabbit β-Gal primary (1:4000, MP Biomedicals) and A488-conjugated anti-rabbit secondary antibodies (1:1000, Molecular Probes) were used. For BrdU immunohistochemistry, tissue sections were pre-treated with 2 M HCl for 1 h at room temperature. Primary antibodies were rat anti-BrdU (1:400, Santa Cruz) and goat anti-DCX (1:500, Santa Cruz) and mouse anti-Mash1 (1:500, BD Biosciences). Colocalization was determined from confocal sections (63× oil objective) of the same SVZs double-immunostained for BrdU and Mash1 or BrdU and DCX.

Blinding of the experiment

After perfusion of the animal, the conditions were blinded by labeling the respective brains with a random combination of letters and handed over to the second experimenter. All data were acquired by providing the second experimenter with only details of how many GCs had to be acquired from each batch of brains to eventually obtain 25 measurements per condition, dpi and domain. This second experimenter was instructed to take only five images per brain for each domain to avoid uneven sampling from single animals. Synaptic densities were quantified for all conditions. Once analysis was completed, we confirmed that all time-points contained 25 neurons per condition (or at least 23 neurons). If it was fewer than 23 neurons, additional neurons were imaged. If it was more than 25 neurons, only the first 25 imaged neurons were included. Once this step was completed, data were unblinded and statistically analyzed.

Morphological analysis

Vibratome sections (150 µm) were incubated with rabbit polyclonal anti-GFP antibody (1:5000) at 4°C for 24 h. Sections were sequentially incubated with biotinylated secondary antibody and with peroxidase-avidin-biotin complex (both biotinylated goat anti-rabbit and ABComplex from Vector Laboratories) and visualized with 3,3′-diaminobenzidine (DAB). Morphological reconstruction of the neurons and their processes was performed using the Neurolucida system (MBF Bioscience) with a

Development (2015) 142, 303-313 doi:10.1242/dev.110767

100× oil-immersion objective (Zeiss Imager). Morphological differentiation was staged based on previously described criteria (Petreanu and Alvarez-Buylla, 2002). The densities of spine-like protrusions were quantified along the distal dendritic tree using a Neurolucida System (100× oil objective). Each protrusion emerging from the dendritic shaft of GFP-labeled GCs was counted as a single protrusion. Neurons were visualized by anti-GFP immunohistochemistry followed by DAB reaction.

Image analysis

Confocal image stacks were acquired using a Leica SPM5 laser scanning microscope (63× oil-immersion lens, 1.4 numerical aperture) (pixel size 0.23×0.23 µm, 512×512 pixel) with a *z*-step of 0.25 µm (80–150 sections). Image acquisition settings of the confocal microscope were initially determined with 28 dpi non-transplanted GCs expressing PSDG and kept constant throughout the study. Maximal intensity projections were used to measure the density of $PSDG^+$ or $SypG^+$ clusters of a dendritic segment with morphometry analysis of ImageJ software. The proximal domain was defined as the first 25 µm of the apical dendrite emerging from the soma. Contact of $PSDG^+$ clusters with the presynaptic marker protein Bassoon was determined in confocal stacks that were imaged as described above. The fluorescent clusters did not overlap in their center, but in their borders. $Bassoon^+$ clusters were located outside the $PSDG^+$ cluster-containing spine. The spines and dendrites of GCs were visualized by immunofluorescence against GFP with a Cy5-tagged secondary antibody. The same results were obtained in these animals by immunofluorescence against the presynaptic marker VGlut1 (anti-guinea-pig antibody, 1:1000, Millipore) where 208 out 210 $PSDG^+$ clusters were contacted by $VGlut1^+$ puncta (supplementary material Fig. S4A).

Electrophysiology

Animals were given an overdose of isoflurane and perfused transcardially with carbonated slicing solution at 4°C containing (in mM) 212 sucrose, 3 KCl, 1.25 NaH_2PO_4, 26 $NaHCO_3$, 7 $MgCl_2$, 0.5 $CaCl_2$ and 10 glucose (306 mOsm, pH 7.3). Bulbs were incubated in ice-cold slicing solution and cut into 350 µm sagittal slices with a vibratome. For recovery, slices were incubated at 32°C for 30 min in carbogenated recording solution containing (in mM) 125 NaCl, 2.5 KCl, 1.25 NaH_2PO_4, 25 $NaHCO_3$, 1 $MgCl_2$, 2 $CaCl_2$ and 25 glucose (312 mOsm, pH 7.3). Fluorescence-guided whole-cell patch clamp recordings were performed with an EPC-10 amplifier (HEKA). The pipette solution contained the following (in mM): 4 KCl, 140 K-gluconate, 10 HEPES, 4 ATP-Mg, 0.3 GTP-Tris and 10 phosphocreatine (292 mOsm, pH 7.2). Lucifer yellow (Sigma) was added to pipette solution (1 mg/ml). Access resistance was <20 MΩ, and the liquid junction potential was not corrected. Resting membrane potential was determined shortly after establishing the whole-cell configuration. Membrane capacitance and resistance were determined by application of a hyperpolarizing pulse. The action potential firing pattern was determined by incremental current steps. Between steps, no current was injected. sEPSCs were recorded in presence of 10 µM gabazine and blocked by 10 µM 6-cyano-7-nitroquinoxaline-2,3-dione (CNQX) at the end of the recording (data not shown). Ten minutes of continuous sEPSC recordings were analyzed with Matlab (The MathWorks) and IgorPro (Wavemetrics) with Taro Tools (Dr Taro Ishikawa, Jikei University School of Medicine Tokyo, Japan). Electrical stimulation was performed with unipolar glass electrodes either in the external plexiform layer or GC layer at 20-50 µm distance from the soma. The evoked EPSCs were averaged, the rise time was determined between 20-80% of the EPSC amplitude and the decay time derived from a fit with a mono-exponential function.

Statistical analysis

Unless otherwise indicated, data were plotted as mean±s.e.m. and analyzed by ANOVA and post-hoc test with Bonferroni correction for multiple comparisons. For pairwise comparisons, Student *t*-test or non-parametric Mann-Whitney test were used. Synaptic densities were approximately normally distributed (Kolmogorov-Smirnov test, $P>0.1$).

Acknowledgements

We thank Dr Carlos Lois for discussions and Cathy Huber for technical support.

Competing interests

The authors declare no competing financial interests.

Author contributions

N.R., Z.L., L.-L.O. and W.K. designed and performed the experiments and analyzed data, K.S. and D.B. contributed reagents, N.R. and W.K. wrote the manuscript.

Funding

The project was funded by a Deutsche Forschungsgemeinschaft (DFG) Emmy-Noether-Grant [KE1661/1-1 to W.K.].

Supplementary material

Supplementary material available online at
http://dev.biologists.org/lookup/suppl/doi:10.1242/dev.110767/-/DC1

References

Bardy, C., Alonso, M., Bouthour, W. and Lledo, P.-M. (2010). How, when, and where new inhibitory neurons release neurotransmitters in the adult olfactory bulb. *J. Neurosci.* **30**, 17023-17034.

David, L. S., Schachner, M. and Saghatelyan, A. (2013). The extracellular matrix glycoprotein tenascin-R affects adult but not developmental neurogenesis in the olfactory bulb. *J. Neurosci.* **33**, 10324-10339.

El-Husseini, A. E., Schnell, E., Chetkovich, D. M., Nicoll, R. A. and Bredt, D. S. (2000). PSD-95 involvement in maturation of excitatory synapses. *Science* **290**, 1364-1368.

Gabay, L., Lowell, S., Rubin, L. L. and Anderson, D. J. (2003). Deregulation of dorsoventral patterning by FGF confers trilineage differentiation capacity on CNS stem cells in vitro. *Neuron* **40**, 485-499.

Hack, M. A., Saghatelyan, A., de Chevigny, A., Pfeifer, A., Ashery-Padan, R., Lledo, P.-M. and Götz, M. (2005). Neuronal fate determinants of adult olfactory bulb neurogenesis. *Nat. Neurosci.* **8**, 865-872.

Hinds, J. W. and Hinds, P. L. (1976). Synapse formation in the mouse olfactory bulb. I. Quantitative studies. *J. Comp. Neurol.* **169**, 15-40.

Kelsch, W., Mosley, C. P., Lin, C.-W. and Lois, C. (2007). Distinct mammalian precursors are committed to generate neurons with defined dendritic projection patterns. *PLoS Biol.* **5**, e300.

Kelsch, W., Lin, C.-W. and Lois, C. (2008). Sequential development of synapses in dendritic domains during adult neurogenesis. *Proc. Natl. Acad. Sci. USA* **105**, 16803-16808.

Kelsch, W., Lin, C.-W., Mosley, C. P. and Lois, C. (2009). A critical period for activity-dependent synaptic development during olfactory bulb adult neurogenesis. *J. Neurosci.* **29**, 11852-11858.

Kelsch, W., Sim, S. and Lois, C. (2010). Watching synaptogenesis in the adult brain. *Annu. Rev. Neurosci.* **33**, 131-149.

Kelsch, W., Sim, S. and Lois, C. (2012). Increasing heterogeneity in the organization of synaptic inputs of mature olfactory bulb neurons generated in newborn rats. *J. Comp. Neurol.* **520**, 1327-1338.

Lemasson, M., Saghatelyan, A., Olivo-Marin, J.-C. and Lledo, P.-M. (2005). Neonatal and adult neurogenesis provide two distinct populations of newborn neurons to the mouse olfactory bulb. *J. Neurosci.* **25**, 6816-6825.

Lepousez, G., Valley, M. T. and Lledo, P.-M. (2013). The impact of adult neurogenesis on olfactory bulb circuits and computations. *Annu. Rev. Physiol.* **75**, 339-363.

Lois, C. and Alvarez-Buylla, A. (1994). Long-distance neuronal migration in the adult mammalian brain. *Science* **264**, 1145-1148.

Lois, C., Hong, E. J., Pease, S., Brown, E. J. and Baltimore, D. (2002). Germline transmission and tissue-specific expression of transgenes delivered by lentiviral vectors. *Science* **295**, 868-872.

Maitra, A., Arking, D. E., Shivapurkar, N., Ikeda, M., Stastny, V., Kassauei, K., Sui, G., Cutler, D. J., Liu, Y., Brimble, S. N. et al. (2005). Genomic alterations in cultured human embryonic stem cells. *Nat. Genet.* **37**, 1099-1103.

Mekhoubad, S., Bock, C., de Boer, A. S., Kiskinis, E., Meissner, A. and Eggan, K. (2012). Erosion of dosage compensation impacts human iPSC disease modeling. *Cell Stem Cell* **10**, 595-609.

Merkle, F. T., Mirzadeh, Z. and Alvarez-Buylla, A. (2007). Mosaic organization of neural stem cells in the adult brain. *Science* **317**, 381-384.

Meyer, M. P. and Smith, S. J. (2006). Evidence from in vivo imaging that synaptogenesis guides the growth and branching of axonal arbors by two distinct mechanisms. *J. Neurosci.* **26**, 3604-3614.

Ming, G.-l. and Song, H. (2011). Adult neurogenesis in the mammalian brain: significant answers and significant questions. *Neuron* **70**, 687-702.

Mori, K. (1987). Membrane and synaptic properties of identified neurons in the olfactory bulb. *Prog. Neurobiol.* **29**, 275-320.

Nikonenko, I., Boda, B., Steen, S., Knott, G., Welker, E. and Muller, D. (2008). PSD-95 promotes synaptogenesis and multiinnervated spine formation through nitric oxide signaling. *J. Cell Biol.* **183**, 1115-1127.

Nissant, A., Bardy, C., Katagiri, H., Murray, K. and Lledo, P.-M. (2009). Adult neurogenesis promotes synaptic plasticity in the olfactory bulb. *Nat. Neurosci.* **12**, 728-730.
Panzanelli, P., Bardy, C., Nissant, A., Pallotto, M., Sassoè-Pognetto, M., Lledo, P.-M. and Fritschy, J.-M. (2009). Early synapse formation in developing interneurons of the adult olfactory bulb. *J. Neurosci.* **29**, 15039-15052.
Petreanu, L. and Alvarez-Buylla, A. (2002). Maturation and death of adult-born olfactory bulb granule neurons: role of olfaction. *J. Neurosci.* **22**, 6106-6113.
Rakic, P., Ayoub, A. E., Breunig, J. J. and Dominguez, M. H. (2009). Decision by division: making cortical maps. *Trends Neurosci.* **32**, 291-301.
Sanes, J. R. (1989). Analysing cell lineage with a recombinant retrovirus. *Trends Neurosci.* **12**, 21-28.
Schönig, K., Weber, T., Frömmig, A., Wendler, L., Pesold, B., Djandji, D., Bujard, H. and Bartsch, D. (2012). Conditional gene expression systems in the transgenic rat brain. *BMC Biol.* **10**, 77.
Sheng, M. (2001). Molecular organization of the postsynaptic specialization. *Proc. Natl. Acad. Sci. USA* **98**, 7058-7061.
Soria-Gómez, E., Bellocchio, L., Reguero, L., Lepousez, G., Martin, C., Bendahmane, M., Ruehle, S., Remmers, F., Desprez, T., Matias, I. et al. (2014). The endocannabinoid system controls food intake via olfactory processes. *Nat. Neurosci.* **17**, 407-415.
Suhonen, J. O., Peterson, D. A., Ray, J. and Gage, F. H. (1996). Differentiation of adult hippocampus-derived progenitors into olfactory neurons in vivo. *Nature* **383**, 624-627.
Taft, C. E. and Turrigiano, G. G. (2014). PSD-95 promotes the stabilization of young synaptic contacts. *Philos. Trans. R. Soc. Lond. B Biol. Sci.* **369**, 20130134.
Valley, M. T., Henderson, L. G., Inverso, S. A. and Lledo, P.-M. (2013). Adult neurogenesis produces neurons with unique GABAergic synapses in the olfactory bulb. *J. Neurosci.* **33**, 14660-14665.
Weinandy, F., Ninkovic, J. and Götz, M. (2011). Restrictions in time and space–new insights into generation of specific neuronal subtypes in the adult mammalian brain. *Eur. J. Neurosci.* **33**, 1045-1054.
Whitman, M. C. and Greer, C. A. (2007). Synaptic integration of adult-generated olfactory bulb granule cells: basal axodendritic centrifugal input precedes apical dendrodendritic local circuits. *J. Neurosci.* **27**, 9951-9961.
Woolf, T. B., Shepherd, G. M. and Greer, C. A. (1991). Serial reconstructions of granule cell spines in the mammalian olfactory bulb. *Synapse* **7**, 181-192.
Yokoyama, T. K., Mochimaru, D., Murata, K., Manabe, H., Kobayakawa, K., Kobayakawa, R., Sakano, H., Mori, K. and Yamaguchi, M. (2011). Elimination of adult-born neurons in the olfactory bulb is promoted during the postprandial period. *Neuron* **71**, 883-897.

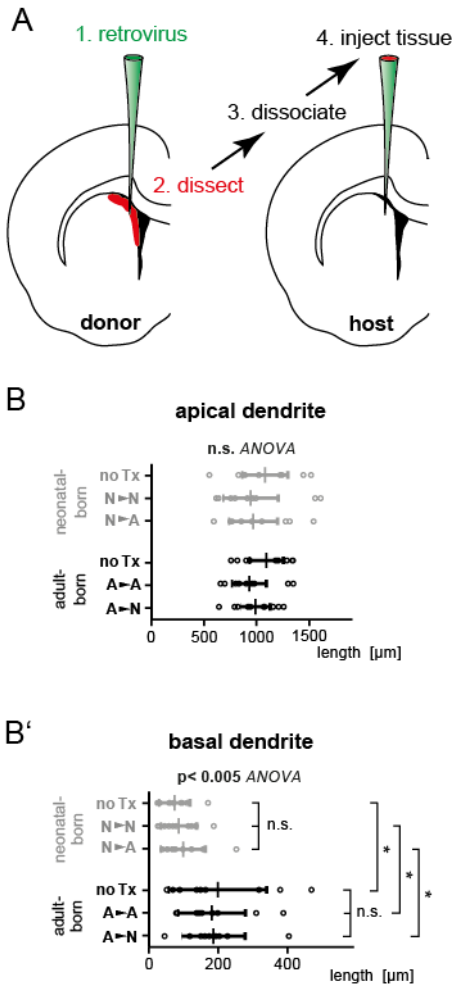

Fig. S1. Transplantation and dendritic length of grafted GCs. (A) Scheme of the transplantation procedure showing the viral injection, dissociation, and transplantation site, respectively. (B-B') Length (mean and 95% confidence interval) of the total apical (B) and basal dendrite (B') of non-transplanted (no Tx) GCs and transplanted GCs at 28 dpi (n=10 GCs per condition, ANOVA followed by posttest (* P<0.05)).

Note: The longer basal dendrites in GCs generated from the adult are explained by the observations that GCs with somata located deeper in the GC layer have longer basal dendrites (e.g. Kelsch et al. (2012) J. Comp. Neurol. 520:1327-38). Importantly, more deep GCs are generated in the adult SVZ. To confirm this observation for transplanted GCs, all neurons in (B') were split into GCs with cell bodies in the lower half of the GC layer (deep GCs) and superficial GCs with somata in the upper half of the GC layer closer to the mitral cell layer. Pooled superficial GCs had similar basal dendrite length independent of whether they were generated from neonatal or adult precursors (65±6 vs. 71±7 µm, n=22 and 6 GCs; n.s., t-test). Similarly, GCs with deep somata generated from neonatal or adult precursors had a similar basal dendrite length (156±18 vs. 221±20 µm, n=8 and 24 GCs; n.s., t-test).

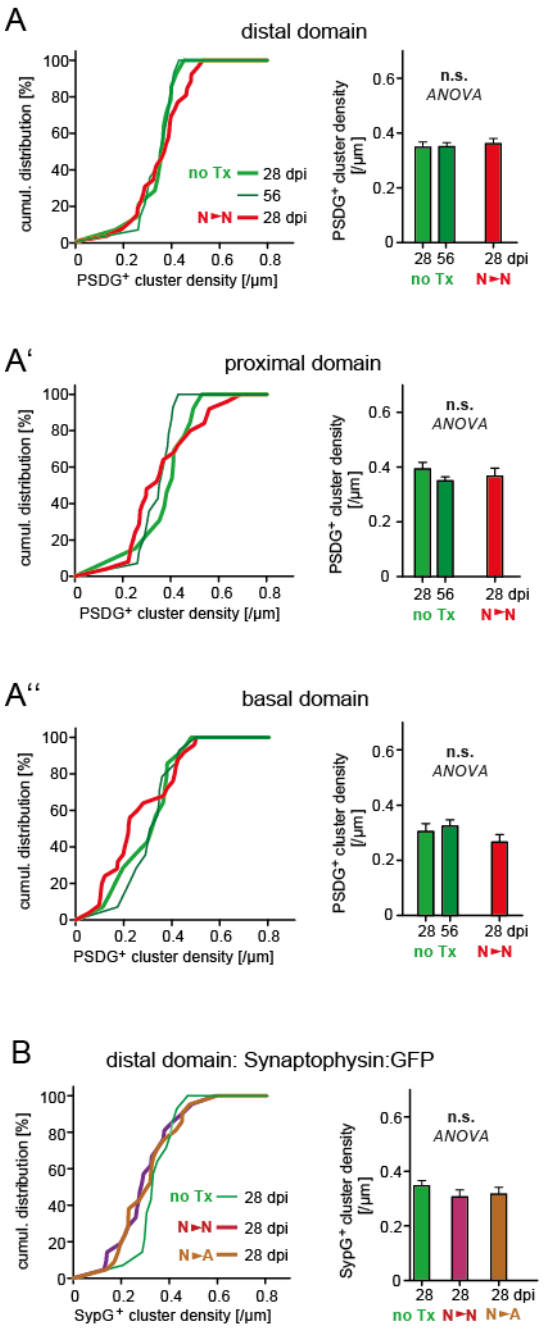

Fig. S2. Organization of glutamatergic input synapses of GCs derived from neonatal precursors. (A-A'') Cumulative plots of PSDG$^+$ cluster densities in the distal (A), proximal (A'), and basal domain (A'') for non-transplanted (no Tx) neonatal-born GCs at 28 and 56 dpi (n=14 GCs for each plotted time point) and the N→N condition at 28 dpi shown in Fig. 4C. Right: Statistical comparison (mean±s.e.m.) of the data shown on the left (ANOVA). (B) Cumulative plots of SypG$^+$ clusters that label presynaptic output synapses in the distal domain of for no Tx neonatal-born, N→N and N→A GCs at 28 dpi (n=14, 25, 25 GCs, respectively). Right: Statistical comparison (mean± s.e.m.) of the data shown on the left (ANOVA).

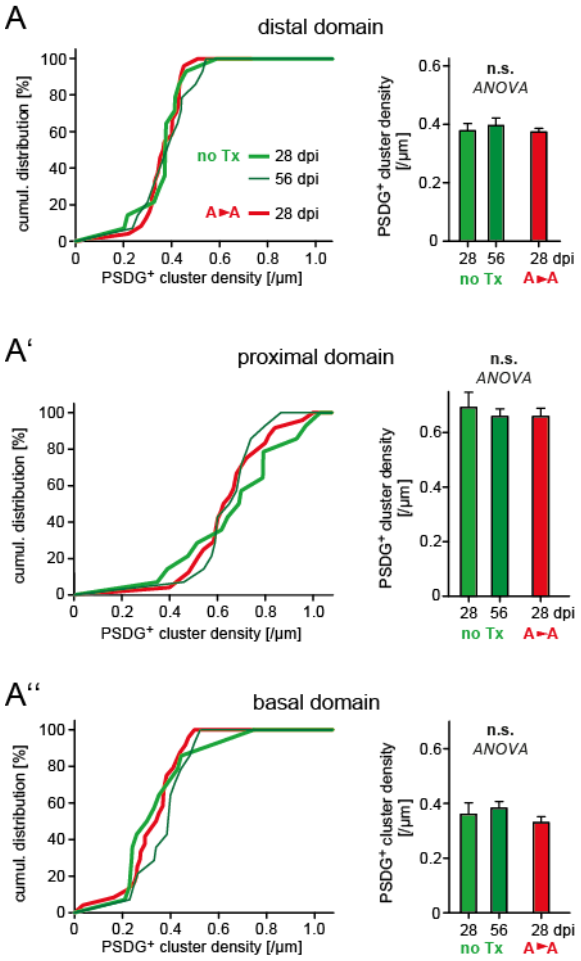

Fig. S3. Synaptic organization of GCs derived from adult precursors. (A-A'') Cumulative plots of PSDG$^+$ cluster densities in the distal (A), proximal (A'), and basal domain (A'') for non-transplanted (noTx) adult-born GCs at 28 and 56 dpi (n=14 GCs, respectively) and the A→A condition at 28 dpi shown in Fig. 5C. Right: Statistical comparison (mean± s.e.m.) of the data shown on the left (ANOVA).

Note: For the data shown in (A), we performed additional analysis for non-transplanted adult-born GCs. In the distal domain, PSDG$^+$ cluster densities tended to increase between 28 and 56 dpi (n.s., t-test), while in the same dendritic segments the density of protrusions tended to decrease (28 dpi: 0.361±0.025/µm and 56 dpi: 0.335±0.023/µm; n=14 GCs, n.s., t-test). However, the difference between the PSDG$^+$ cluster density and the spine density in the same neurons increased significantly from 28 to 56 dpi (28 dpi: 0.016±0.002/µm and 56 dpi: 0.061±0.010/µm; n=14 GCs, p=0.0002, t-test).

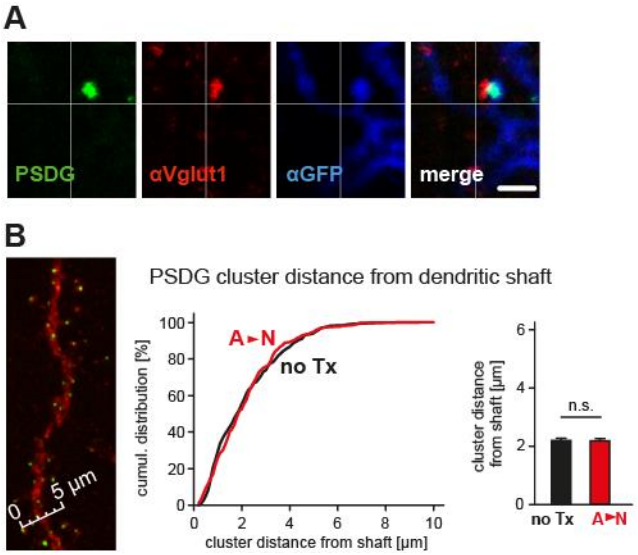

Fig. S4. PSD-95:GFP distribution along distal dendrites of A→N GCs and its presynaptic contact. (A) In the distal domain of A→N GCs at 28 dpi, PSDG$^+$ clusters were contacted by a presynaptic marker, Vglut1 (scale bar 3 µm). (B) Left: Measurement of the distance of PSDG$^+$ clusters from the dendritic shaft in the distal domain in maximum density projection (scale bar 5 µm). Middle: Cumulative plots of the distance of PSDG$^+$ clusters from the dendritic shaft in the distal domain of non-transplanted (no TX) adult-born GCs and A→N GCs at 28 dpi (total number of clusters analyzed: 436 and 315 in 10 GCs, respect.). Right: Statistical comparison (mean± s.e.m.) of the data shown to the left (t-test).